Published in final edited form as:
Mater Sci Eng C Mater Biol Appl. 2014 November 1; 0: 191–200. doi:10.1016/j.msec.2014.08.036.

Surface microcracks signal osteoblasts to regulate alignment and bone formation

Yutian Shu[1,4], **Melissa J. Baumann**[1,3,*], **Eldon D. Case**[1], **Regina K. Irwin**[2], **Sarah E. Meyer**[1], **Craig S. Pearson**[1], and **Laura R. McCabe**[2,*]

[1]Chemical Engineering and Materials Science Department, Michigan State University, East Lansing, Michigan 48824

[2]Physiology and Radiology Departments, Michigan State University, East Lansing, Michigan 48824

[3]Department of Mechanical Engineering, Auburn University, Auburn, Alabama 36849

[4]The College of Materials Science and Engineering, Beijing University of Technology, Beijing 100124, People's Republic of China

Abstract

Microcracks are present in bone and can result from fatigue damage due to repeated, cyclically applied stresses. From a mechanical point, microcracks can dissipate strain energy at the advancing tip of a crack to improve overall bone toughness. Physiologically, microcracks are thought to trigger bone remodeling. Here, we examine the effect of microcracks specifically on osteoblasts, which are bone-forming cells, by comparing cell responses on microcracked versus non-microcracked hydroxyapatite (HA) specimens. Osteoblast attachment was found to be greater on microcracked HA specimens ($p<0.05$). More importantly, we identified the preferential alignment of osteoblasts in the direction of the microcracks on HA. Cells also displayed a preferential attachment that was 75 to 90 μm away from the microcrack indent. After 21 days of culture, osteoblast maturation was notably enhanced on the HA with microcracks, as indicated by increased alkaline phosphatase activity and gene expression. Furthermore, examination of bone deposition by confocal laser scanning microscope indicated preferential mineralization at microcrack indentation sites. Dissolution studies indicate that the microcracks increase calcium release, which could contribute to osteoblast responses. Our findings suggest that microcracks signal osteoblast attachment and bone formation/healing.

*Editorial correspondence and reprint requests to: Laura R. McCabe, Ph.D., Michigan State University, Departments of Physiology and Radiology, Biomedical Physical Science Bldg., 567 Wilson Road, East Lansing, MI 48824, (517) 884-5152, (517) 355-5125 FAX, mccabel@msu.edu. Melissa Baumann, Ph.D., Auburn University, Department of Mechanical Engineering, Auburn, Alabama 36849, MJB0041@auburn.edu.

Keywords

osteoblast; microcracks; attachment; alignment; maturation

1. Introduction

Outside of developmental events, bone forms in response to cracking, which can signal a cascade of events involving osteocytes (OCy), osteoblasts (OB) and osteoclasts (OC) [1-5]. Cracks can result from fatigue damage due to repeated, cyclically applied stresses [2,6-8]. Microcracks are common in greyhounds [2], horses [9], and human athletes, especially runners [10]. For example, Muir *et al*. found linear microcracks in the fatigue fracture of the central tarsal bone in racing greyhounds [2]. The tip-to-tip lengths of the resulting linear microcracks range from approximately 50 to 300 μm [3, 11-13]. From a mechanical standpoint, the formation of microcracks in the vicinity of fatigue fracture [2, 6, 11, 14] may prevent catastrophic bone failure by dissipating strain energy at the advancing crack tip, thereby improving the overall bone toughness [15,16].

From a physiologic standpoint, microcracks play an important role in triggering bone healing and/or bone remodeling when the bone is adapting to an externally applied stress [2-5]. Bone remodeling is an interactive process where OCs resorb existing bone, OBs form new bone, and OCys regulate bone homeostasis [17-20]. Microdamage can induce OCy apoptosis, which promotes OC recruitment for targeted resorption [21, 22]. However, microdamage may also promote OB activation through several mechanisms, including through the release of matrix embedded growth factors such as TGF-beta, bone morphogenic proteins (BMPs), IGFs, and PDGF, which are known to stimulate OB growth and maturation. With regard to the chemical environment, microcracking alters surface topology and increases mineral dissolution into the surrounding medium. These minerals are predominantly calcium and inorganic phosphate ions [23]. Calcium ion signaling is known to control OB growth and differentiation in bone and Sun *et al.* have shown that bone matrix calcium efflux generated by mechanical stretch stimulates OB response at the stretch concentration site [23]. Likewise, in HA, dissolution leads to release of calcium and inorganic phosphate ions.

To examine the effects of microcracks directly on OB attachment, alignment, growth, maturation, and mineralization, we measured OB cellular responses to microcracking in biomimetic HA bone scaffolds.While bone cracking is a dynamic event resulting from overloading, crack repair occurs in the absence of or at most, under a minimal load [2]. Therefore, no loading was applied to the HA scaffolds used for this study. Using the HA scaffolds, rather than bone matrix, allowed us to isolate the effects of microcracks without the influence of released bone matrix proteins or other cellular materials. Using a solid surface removed the influence of porosity, which many other researchers have shown to be key in OB attachment [24]. Our results show that microcracks act as a primary influence on OBs.

2. Materials and methods

2.1 HA specimen preparation

Following established procedures, HA powders (Taihei, Osaka, Japan) with particle size 4-6 μm were uniaxially pressed in a 32-mm diameter steel pellet die at 28 MPa for one minute. The green HA specimens were subsequently sintered in air at 1360°C for 4 h and polished down to 0.5 μm grit size with diamond paste. Microcracks were introduced to the polished surfaces using Vickers indentation with a Shimadzu micro-hardness tester at 4.9 N. Indents were introduced in a 7×7 grid with a 2 mm interval as shown schematically in Figure 1. This crack interval was chosen to be more than 10 times the crack length (150 μm) to avoid any possible interactions between neighboring cracks.

2.2 HA characterization

2.2.1 X-ray Diffraction—The phase purity of HA, both as-received powder and pulverized powder from sintered HA specimens was determined by X-ray diffraction (XRD) using Bruker D2 Phaser diffractometer equipped with Cu KαX-ray radiation operating at 30 kV, 10 mA and at sweep rates of 0.5° 2θ /min. The sample placed in a PMMA sample holder was rotated at 5°/min.

2.2.2 Microscopy—The surface morphology of both microcracked and non-microcracked HA surfaces were imaged using a scanning electron microscope (SEM) (JEOL-6400V SEM, JEOL Ltd., Japan) and confocal laser scanning microscope (CLSM) (Zeiss LSM 5 Pascal, Carl Zeiss, Inc., Thornwood, NY). Prior to SEM imaging, HA disks were coated with gold.

2.3 Cell culture

Following procedures established in our laboratory [25, 26], MC3T3-E1 mouse OB cells were seeded at a density of 11,320/cm^2 for the evaluation of cell attachment and growth.The cell passage number is controlled at around 23 to guarantee consistent and comparable cell behavior between control and experimental groups.For cell maturation studies, cells were seeded at a density of 20,000/cm^2. Cells were fed every other day with α-MEM media supplemented with 10% fetal bovine serum (FBS), 100 units Penicillin and 100 μg Streptomycin and cultured in a humidified atmosphere containing 95% air and 5% CO_2 at 37°C. The media was further supplemented with 2 mM inorganic phosphate and 2.5 μg/mL ascorbic acid to promote differentiation when cells reached confluence [25].

2.4 Osteoblast attachment and growth

Cell attachment was evaluated at 1, 2 and 4 h while cell growth was evaluated at 1, 3 and 5 days. Three specimens were used for each condition and the experiments were tripled. At the given time points, cells were fixed and stained with Hoechst 33342, and cell numbers counted using Cell Profiler. The relative fractions of attachment and growth were calculated by normalizing the cell density at each time period with the initial seeding density.

2.5 Osteoblast maturation

Cells were cultured on microcracked and non-microcracked HA disks for 21 days. To assess the level of maturation in the culture, staining was carried out to assess extracellular matrix and mineralization. Alkaline phosphatase (AP) staining was performed by incubating the OBs for 30 minutes at 37°C with 0.5 mg/mL naphthol AS-MX phosphate disodium salt with 1 mg/mL Fast Red TR salt in a 10.2 M Tris buffer, pH 8.4. AP quantization was performed by solubilizing the precipitated salt in 100% TCA, diluting 1:10, and reading at 540 nm as previously described [27].

For molecular analyses of maturation and gene expression, RNA was isolated from OBs harvested from non-microcracked and microcracked HA at 21 days, using Tri Reagent (Molecular Research Center, Inc., Cincinnati, OH). RNA integrity was assessed by formaldehyde-agarose gel electrophoresis. cDNA was synthesized by reverse transcription with Superscript II Reverse Transcriptase Kit and oligod$T_{(12\text{-}18)}$ primers (Invitrogen, Carlsbad, CA) and amplified by real-time PCR with iQ SYBR Green Supermix (Biorad, Hercules, CA) and gene-specific primers for Runx2 and alkaline phosphatase [28]were synthesized by Integrated DNA Technologies (Coralville, IA). Hypoxanthine guanine phosphoribosyltransferase (HPRT) mRNA levels do not fluctuate between conditions and were used as an internal control. Other primers used are previously described [29, 30].

2.6 CLSM imaging of osteoblasts

OBs on microcracked and non-microcracked HA specimens were stained with Rhodamine Phalloidin actin and Hoechst nucleus stain and imaged using CLSM (Olympus FluoView, Tokyo, Japan). At four hours, a total of 30 micrographs were collected for both the control (non-microcracked) and the experimental (microcracked groups), with at least 500 cells analyzed per condition.

Xylenol Orange powder (Sigma-Aldrich Co., St. Louis, MO) was dissolved in distilled water to make a 20 mM stock solution which was added to differential media for detecting calcium formation [31]. Mineralization was assessed by pulsing the culture with 20 μM Xylenol Orange and then visualizing the disk using CLSM (Olympus FluoView, Tokyo, Japan).

2.7 HA dissolution

Both the polished non-microcracked specimens (control group) and indented specimens (experiment group) were maintained at 37°C and immersed in distilled water to address the question if the microcracks were sufficient to induce dissolution and to reduce the background of other cation and anion effects on our measurements. The immersion periods ranged from one hour to 7 days (1, 1.5, 2, 3, 4, 6, 8, 13 and 18 h and 1, 2, 3, 4, 5 and 7 days). HA dissolution was characterized by measuring the calcium ion (Ca^{2+}) concentration in distilled water sampled at each time interval using atomic absorption spectrophotometry (AAS, model 3110, PerkinElmer, Massachusetts, 0.01 mg/L) where the emission light wavelength for Ca^{2+} is 422.7 nm.

2.8 Statistics

Student's t-test was used to test the statistical significance of the differences where a value of $p < 0.05$ was considered significant.

3. Results

3.1 HA characterizationfor osteoblast studies

The XRD analysis of as-received HA powder and pulverized sintered HA specimen showed that both HA powders were crystalline with characteristic peaks matching with the standard JCPDS 9-432 (Joint Committee on Powder Diffraction Standards, Swarthmore, PA). No phases other than HA were detected (Figure 2). Both the SEM and CLSM images of non-microcracked HA showed a smooth surface with uniformly distributed, isolated, surface-breaking pores approximately 3 μm in diameter (Figure 3A and 3C). The SEM image of the microcracked HA specimens clearly showed both the indentation impressions and chipping at the vicinity of the indentation impression (Figure 3B). The CLSM image of microcracked HA showed radial cracks aligned parallel to the indentation diagonal as well as quarter plate like lateral cracks (Figure 3D).The average size of the lateral cracks, *b*, and the half radial crack length, *a*,on HA, were 67.3 ± 17.5 μm and 90.6 ± 4.9 μm, respectively (Figure 1A). Compressive fracture strength did not significantly differ between noncracked and microcracked discs (data not shown).

3.2 Osteoblastattachment and alignment

Cell attachment was visualized by fluorescent microscopy and staining with Hoechst 33342 (to visualize nuclei, blue) and Rhodamine Phalloidin(to visualize actin cytoskeleton, red) (Figure 4A). At one and two hours post seeding, OBs were round and not fully attached to either HA surface, but by four hours the cells began to elongate. A significant increase of OB attachment onto microcracked HA specimens was observed at four hours ($p<0.05$), but not at earlier hours(Figure 4B).

CLSM fluorescent micrography of cells attached on microcracked HA at four hours post-seeding demonstrates the alignment of the elongated cells towards the indentation center, described by the alignment angle, θ, as shown in Figure 5A. For the few circular cells (cells that were not fully attached), no alignment angle could be defined. These cells were thus excluded from the quantitative angular distribution analysis for non-cracked and microcracked surfaces (8% versus 3% excluded, respectively).

For the CLSM micrographs of the HA specimens, the alignment angle, θ, for the elongated cells, the coordinates of the crack center O (X_0, Y_0) and the cell nucleus center C (X, Y) were determined via the software package Datathief [32]. The vector $\overrightarrow{OC} = (X - X_0, Y - Y_0)$ then gave the relative position of each cell with respect to the indentation center. For each cell, the elongation direction was described by another vector, $\overrightarrow{EF} = (X_2 - X_1, Y_2 - Y_1)$, where E ($X_1$, Y_1) and F (X_2, Y_2) are two points along the elongated cell filaments. The angle, θ, can then be calculated from equation (1),

$$\theta = arc|cos\theta| = arc|\left(\overrightarrow{OC} \bullet \overrightarrow{EF}\right) / \left(|\overrightarrow{OC}||\overrightarrow{EF}|\right)| \quad (1)$$

For the non-microcracked (control) HA specimens, no Vickers indentations were made. Thus, in order to define the angle of alignment for cells on non-microcracked HA, artificial origins of polar coordinate system were superimposed on the CLSM micrographs of the non-microcracked HA specimens. These artificial origins were superimposed near the center of micrographs for non-microcracked HA specimens, similar to the positions of the indentation centers on micrographs of microcracked HA.

The alignment angle, θ, of cells rangedfrom 0° to 90° with respect to the microcracked region centered at the indentation center, as shown schematically in Figure 5B. Figure 6 shows the probability density histograms of θ (probability versus θ) for the elongated cells measured from the CLSM micrographs of both the non-microcracked and the microcracked HA. The distributions of the angle θ were then compared to a uniform distribution described by equation (2),

$$f(\theta) = \frac{1}{(b-a)}, a < \theta < b \quad (2)$$

where *a* and *b* are the two parameters for a uniform distribution and give the range of angle θ. The goodness of fit was determined using the Kolmogorov-Smirnov method [33].The uniform distribution of angle θ corresponds to the random cell orientations with respect to the origin of the polar coordinate system [34, 35]. The θ distribution was uniform for OBs on the non-microcracked HA ($p>0.05$) (Figure 6A), but non-uniform ($p<0.05$) for OBs on the microcracked HA (Figure 6B).

Next, we compared the aligned to non-aligned cells. When θ is less than 45°, the midpoint of the [0°, 90°] interval, cells with θ < 45° are considered to be aligned towards the microcracked region (Figure 5B). To determine whether the OBs on the microcracked HA specimens aligned in the direction of the microcracked zone, the cells were divided into three groups according to both their alignment angle and shape: (i) aligned cells (θ < 45°), (ii) non-aligned cells (θ ≥ 45°) and (iii) circularcells for which alignment was indeterminate. On the non-microcracked HA specimens, the relative fraction of aligned cells (θ < 45°) was significantly less ($p<0.05$) than the relative fraction of non-aligned cells (θ ≥ 45° and circular cells) (Figure 6C). In contrast, the relative fraction of aligned cells (θ < 45°) was significantly more ($p<0.05$) than non-aligned cells (θ ≥ 45° and circular cells) on the microcracked HA specimens as shown in Figure 6D.

The location/position of the aligned cells (θ < 45°) was characterized by the distance (r) between each cell nucleus and the indentation center, which was obtained by calculating the length of vector $\overrightarrow{OC} = (X - X_0, Y - Y_0)$ described in section 4.2 using equation (3),

$$r = |\overrightarrow{OC}| = \sqrt{(X - X_0)^2 + (Y - Y_0)^2} \quad (3)$$

The micrographs of the microcracked HA surface were then partitioned into a circle centered at the indentation site, with increasing concentric 15 μm-wide annuli as shown schematically in Figure 7A. The center circle has an area of 706.85 μm^2, and the n^{th}(n=1, 2…) annulus has an area of $\pi[15(n+1)]^2$-$\pi(15n)^2$ (μm^2). The number of aligned cells within the central circle and each ring was then normalized by the circle/annulus area to yield the cell density as a function of distance away from the indentation center (Figure 7B).

The surface microcracked zone introduced using Vickers indentation contains the indentation impression, lateral cracks and radial cracks. The average lateral crack size and the half radial crack length were approximately 67.3 ± 17.5 μm and 90.6 ± 4.9 μm, respectively. The boundary region of the microcracked zone as determined by both lateral and radial cracks is thus an annulus approximately 67.3μm to 90.6 μm away from the indentation center. The highest density of aligned cells was found in the ring located 75 μm to 90 μm from the indentation center (Figure 7B). This concentric ring was similar in size to the boundary region of the microcracked zone determined by the lateral and radial cracks.

3.3 Osteoblastgrowth and maturation

No significant differences in OB number were detected between microcracked and non-microcracked specimens at one, three and five days post-seeding (Figure 8), suggesting that OB growth was similar on both surfaces, despite early differences in OB attachment. While we could not measure the rate of maturation (due to disc limitations), we did examine the effect of microcracking on OB phenotype markers at one time point, 21 days post-seeding, which is a time point commonly used to detect expression of genes associated withOB maturation. Our study demonstrated that there are indeed differences inOBgene expression between non-cracked and microcracked surfaces. . Cells on the microcracked surface had greater AP mRNA levels and correspondingly greater AP activity compared to non-microcracked surfaces (Figure 9), both are markers of mid-to-late stage extracellular matrix maturation [36-38]. Further analysis indicated an increase in mRNA levels of Runx2, a transcription factor important for OB lineage selection and maturation (Figure 9). No significant changes were observed in expression of markers of late stage OB maturation, such as osteocalcin (not shown)[36-38].

To determine if the identified phenotypic changes are associated with altered OB mediation of bone formation on the microcracked HA surface, we imaged OB mineralization on microcracked and non-microcracked HA at 21 days by CLSM. Surface analyses indicated that significantly more mineral deposition occurred on the microcracked HA. The deposited minerals, were visualized by Xylenol Orange stain pulsing, and appeared as orange dots (Figure 10). Non-microcracked HA (Figure 10A) displayed mineral deposition that was scattered uniformly across the surface. In contrast, there was a zone of concentrated mineral deposition at the indentation site on the microcracked HA (Figure 10B). The concentrated mineral deposition was not apparent in parallel studies on microcracked and non-microcracked HA scaffolds incubated for the same time without cells (data not shown).These results suggest that HA cracking stimulates OB mediated bone formation at sites of surface indentations, perhaps in an effort to repair and smooth the surface.

3.4 Calcium ion concentration measurement and calculation of surface area increase

Figure 11 shows that the calcium ions released from both non-microcracked HA (○) and microcracked HA (□) increased exponentially with immersion time in distilled water. The data from both the non-microcracked and the microcracked HA specimens were fit to equation (4) via a least squares technique,

$$C = C_s - (C_s - C_0)\, exp\,(-t/\tau) \quad (4)$$

where C is the calcium ion concentration released into distilled water from microcracked HA, t is the immersing time, C_s corresponds to the plateau value of calcium concentration at $t \to \infty$, C_0 corresponds to the calcium concentration in distilled water at $t=0$, and τ is a time constant that inversely correlates to the changing rate of calcium ion concentration.

The least squares fit for non-microcracked HA yields $C_s = 14.38 \pm 0.26$ mg/L, C_0-$C_s = -13.64 \pm 0.31$ mg/L (such that C_0 is approximately 0.74 mg/L), and $\tau = 23.74 \pm 0.003$ h, with a coefficient of determination, R^2 of 0.994. The least squares fit of the microcracked HA data yields $C_s = 15.32 \pm 0.18$ mg/L, C_0-$C_s = -15.11 \pm 0.30$ mg/L (such that C_0 is around 0.21 mg/L), and $\tau = 12.01 \pm 0.004$ h, with a coefficient of determination, R^2 of 0.996.

Besides the changes in HA dissolution behavior, the introduction of Vickers indentation can also lead to slight surface area increases. The surface area resulting from Vickers indentation impression can be calculated using equation (5),

$$\mathrm{A} \approx \mathrm{d}^2/1.8544 \quad (5)$$

where A is the surface area, d is the indentation diagonal [ASTM E384-11]. When compared to a 2D square with diagonal d, which has a surface area of $d^2/2$, the relative increase in surface area[1] is approximately 8%. In the current study, the indentation diagonal d is approximately 45 μm, and the increase in surface area from each indentation can be calculated to be 79.5 μm^2. The total increase in surface area from the 7×7 indentation grid is thus approximately 3,900 μm^2, which when compared to the non-microcracked surface area represents a fractional increase in area of only 9×10^{-6}. Furthermore, it is worth noting that elastic recovery resulting from Vickers indentation will act to decrease the added surface area. While the overall increase, even without accounting for elastic recovery, is very small in this case(1 part in 100,000), the effect of elastic recovery on surface area of Vickers indentation should not be dismissed [39-41].

4. Discussion

4.1 Osteoblast attachment and growth

Attachment or adhesion, being the first phase of OB/substrate interaction, plays an important role in determining the subsequent proliferation and differentiation stages [42]. In this study, the presence of microcracks was observed to increase OB attachment four hours after seeding. We further show that within 4 h, calcium dissolution occurs from the HA disks with

[1] $(d^2/1.8544 - d^2/2)/(d^2/2) \approx 0.08$

microcracks. While surface topology and roughness have been shown to regulate OB attachment [43], increased extracellular calcium ions are also known to impact OB behavior [23, 44]. Interestingly, while attachment was enhanced on microcracked HA, it did not affect OB proliferation. Smith *et al.* reported a similar finding in a study examining OBs cultured on HA [26].

Perhaps more interesting is that the actual cell alignment, upon attachment, appears to reflect the cell's response to the substrate surface, such that the formation of cytoskeletal focal adhesions is guided by the substrate physical/chemical properties in order to optimize cell functions on the substrate [45]. The uniform distribution of cell alignment angles, θ, on non-microcracked HA specimens indicated that the OBs were randomly oriented and showed no preferential alignment towards the superimposed polar coordinate origins. The random orientation of the elongation axes for the cells also implies a random movement of cells on the non-microcracked HA surfaces. The non-uniform distribution of the cell alignment angles (θ) on microcracked HA showed that the presence of the microcracks introduced by Vickers indentation affected the cell orientation.

In an *in vivo* study by Frost, microcracks were observed to lead down to spaces containing cells and/or capillaries indicating an ongoing repairing process [46]. In our current *in vitro* study, the cell alignment towards the microcracked zone was noted specifically at the crack boundaries, suggesting the initiation of a repairing process through mineral deposition, which was observed later at 21 days. The introduction of microcracks could disturb the local physical/chemical environment(as shown by more calcium release) which in turn can alter the cell elongation direction when the cells were attaching in the vicinity of the microcracked zone. It is worthwhile to note that when microcracking occurs *in vivo*, OBs do not necessarily have direct contact with the microcracked sites, but may be generated and migrate from the undamaged bone before mineralizing in the vicinity of the microcracks [47]. The microcracked zone introduced using Vickers indentation is localized microdamage, mimicking the localized damage found from repetitive use injury in humans and animals [3, 12,47].

The observed OB alignment at the periphery of the microcracked zone suggests two possible bone-healing processes, identified by examining both the radial and lateral cracks. The first is that crack tip blunting may be activated at the radial crack tips. This resembles bone healing in the case of fatigue microcracking *in vivo* as observed by Muir [2], Zarrinkalam [6], O'Brien [7] and Hazenberg [8]. The second is the possible inhibition of lateral crack chipping that could occur in bone *in vivo*, a concept that has yet to be addressed in the literature.

4.2 Osteoblastmaturation and mineralization

In this study we found that OBs cultured on microcracked HA displayed increased markers of early stage maturation, including Runx2 and alkaline phosphatase, after 21 days of growth on the HA discs. Runx2 is critical for OB maturation while alkaline phosphatase is essential for normal mineralization through its ability to generate free phosphate from pyrophosphate [36-38]. Thus,our data supports that microcracks stimulate expression of genes required for bone healing, which is consistent with our identification of increased

mineralization at microcrack regions. While we did not observe an elevation of late stage OB maturation markers (osteocalcin), it is possible that we would observe a microcrack-induced increase in osteocalcin at a later time point or alternatively the OB response to micro-cracks is gene specific. Due to the extensive time to microcrack HA discs and our choice to not reuse the discs (after an experiment), we were limited by the number of discs and unable to examine later time points. The increased gene expression that we observed *in vitro* suggests that the introduction of microcracks has the potential to enhance bone healing *in vivo*.

4.3 HA dissolution

Microcracking inherently forms two new surfaces, leading to an increase in surface area and mineral dissolution into the surrounding medium. In the case of bone matrix, these minerals are predominantly calcium and inorganic phosphate ions [23]. The release of both calcium and phosphate ions can influence bone cell responses and matrix mineralization *in vitro* [48-55]. Calcium is known to regulate OB growth and differentiation [23, 55] and is sensed by OBs through calcium sensing receptors and calcium channels that ultimately modify intracellular signaling to affect maturation and bone formation [55]. Our studies demonstrate that the concentration of calcium ions released from microcracked HA rises significantly higher compared to non-microcracked HA at four hours. The calcium release rate from themicrocracked HA surface is faster than that from non-microcracked HA surfaces as indicated by the time constant τ, which is inversely correlated to the calcium ion release rate, such that the smaller the value of τ, the faster the release rate. For non-microcracked HA, $\tau = 23.74 \pm 0.003$ h, which is about twice the value for the time constant for the microcracked HA, where $\tau = 12.01 \pm 0.004$ h. Both the higher calcium concentration and the faster calcium release rate from the microcracked HA surface shows that the dissolution of the HA surface was enhanced by the presence of indentation and associated microcracks. This introduction of Vickers indentation impressions is associated with a negligible increase in overall surface area. However, upon the introduction of Vickers indentation on HA, a residual compressive strain energy reservoir will form beneath the indentation impression [56-58], and the strain energy could be released through radial crack propagation [59], lateral crack expansion and possibly subsequent surface spalling [60], as well as surface dissolution [61]. A study by Li *et al*. showed that the indentation damage and crack edges in bioglass experienced faster dissolution than the undamaged areas [61]. Similarly, the local damage caused by Vickers indentation in HA could lead to the observation of significant overall increase in calcium ion release from the microcracked HA surface which, based on past reports showing that calcium enhances OB activity, suggests that the OB responses we observe are likely a result of the differential and enhanced ion release from the microcracked HA surface rather than from the negligible change in the surface area (less than the fractional increase of 9×10^{-6}).

Also, it is worth noting that surface polishing of HA in this study should not be confused with surface abrasion used in many other studies [62, 63]. Typically surface abrasion produces surface corrugation and/or cracks [64, 65]. However, in this study surface polishing was done with a series of grit sizes ending with 0.5 μm grit, at which stage the surface corrugation is very limited. Also, the load applied when polishing is likely below the pop-in threshold for cracks for fine polishing grit acting as sharp “indenters” [66].

Moreover, HA specimens used as the control and experimental groups went through the same polishing procedure and have comparable surfaces; thus it is unlikely that the altered cell behaviors observed for microcracked HA is associated with surface polishing.

5. Conclusion and future directions

Our studies establish that introduction of microcracks onto HA surfaces promotes OB alignment, enhances OB attachment and maturation, and has the potential to ultimately improve the rate of bone healing. Based on this, it is reasonable to postulate that the inclusion of microcracks could improve the design of a bone tissue engineered scaffold. It should be noted that microcracks could weaken a scaffold, though we did not observe this in our study. The preferred use of implants made of porous ceramic scaffolds/coatings over strong metallic materials is based on the necessity for implant-bone integration rather than increaseing load-bearing function, especially because all bone repairs require mechanical stabilization. The observed increase in attachment and preferential alignment of OBs to the microcracked zone may promote localized mineralization, and therefore could direct bone formation at specific scaffold sites in future implants. Based on our studies and the literature, it appears that the calcium ion concentration changes within the microenvironment of the microcracks direct targeted OB responses to microcracks. Thus, the physiologic benefits of such cracks bring a new dimension to designing scaffolds for bone tissue engineering. The optimal microcrack size, size distribution, and/or the microcrack density still require further investigation.

Acknowledgments

The authors acknowledge the financial support from National Science Foundation Grant DMR-0706449, and the technical support for using confocal laser scanning microscope from Center for Advanced Microscopy of Michigan State University. LRM is also funded by National Institute of Health, DK101050 and AT007695.

References

1. Nakamura I, Takahashi N, Jimi E, Ugadawa N, Suda T. Regulation of osteoclast function. Modern Rheumatology. 2012; 22(2):167–177. [PubMed: 21953286]
2. Muir P, Johnson KA, Ruaux-Mason CP. *In vivo* matrix microdamage in a naturally occurring canine fatigue fracture. Bone. 1999; 25:571–576. [PubMed: 10574577]
3. Mori S, Burr DB. Increased intracortical remodeling following fatigue damage. Bone. 1993; 14:103–109. [PubMed: 8334026]
4. Prendergast PJ, Taylor D. Prediction of bone adaptation using damage accumulation. J Biomech. 1994; 27:1067–1076. [PubMed: 8089161]
5. Taylor D. Bone maintenance and remodeling: A control system based on fatigue damage. J Orthop Res. 1997; 15:601–606. [PubMed: 9379271]
6. Zarrinkalam KH, Kuliwaba JS, Martin RB, Wallwork MA, Fazzalari NL. New insights into the propagation of fatigue damage in cortical bone using confocal microscopy and chelating fluorochromes. Eur J Morphol. 2005; 42:81–90. [PubMed: 16123027]
7. O'Brien FJ, Taylor D, Lee TC. Microcrack accumulation at different intervals during fatigue testing of compact bone. J Biomech. 2003; 36:973–980. [PubMed: 12757806]
8. Hazenberg JG, Hentunen TA, Heino TJ, Kurata K, Lee TC, Taylor D. Microdamage detection and repair in bone: Fracture mechanics, histology, cell biology. Technol Health Care. 2009; 17:67–75. [PubMed: 19478407]

9. Esterberg L, Stover SM, Gardner A, Drake CM, Johnson B, Ardans A. High speed exercise history and catastrophic racing fracture in thoroughbreds. Am J Vet Res. 1996; 57:1549–1555. [PubMed: 8915427]
10. Burr DB. Bone, exercise and stress fractures. Exerc Sport Sci R. 1997; 25:171–194.
11. Burr DB, Milgrom C, Boyd RD, Higgins WL, Robin G, Radin EL. Experimental stress fractures of the tibia, Biological and mechanical aetiology in rabbits. J Bone and Joint Surg. 1990; 72B:370–375.
12. Burr DB, Martin RB. Calculating the probability that microcracks initiate resorption spaces. J Biomech. 1993; 26:613–616. [PubMed: 8478363]
13. Lee TC, Myers ER, Hayes WC. Fluorescence-aided detection of microdamage in compact bone. J Anat. 1998; 193:179–184. [PubMed: 9827633]
14. Radtke CL, Danova NA, Scollay MC, Santschi EM, Markel MD, Gomez TD, et al. Macroscopic changes in the distal ends of the third metacarpal and metatarsal bones of thoroughbred racehorses with condylar fractures. Am J VetRes. 2003; 64:1110–1116.
15. An B, Liu Y, Arola D, Zhang D. Fracture toughening mechanism of cortical bone: An experimental and numerical approach. J MechBehav Biomed. Article in Press.
16. Taylor D, Prendergast PJ. Damage accumulation in compact bone – a fracture mechanics approach to estimate damage and repair rates. AdvBioeng. 1995; 13:337–338.
17. Atkins GJ, Findlay DM. Osteocyte regulation of bone mineral: A little give and take. Osteoporosis Int. 2012; 23(8):2067–2079.
18. Cowin SC, Hegedus DH. Bone remodeling I: theory of adaptive elasticity. J Elasticity. 1976; 6:313–326.
19. Verborgt O, Gibson GJ, Schaffler MB. Loss of osteocyte integrity in association with microdamage and bone remodeling after fatigue in vivo. J Bone Miner Res. 2000; 15:60–67. [PubMed: 10646115]
20. Rumpler M, Würger T, Roschger P, Zwettler E, Peterlik H, Fratzl P, Klaushofer K. Microcracks and osteoclast resorption activity in vitro. Calcif Tissue Int. 2012; 90(3):230–238. [PubMed: 22271249]
21. Colopy SA, Benz-Dean J, Barrett JG, Sample SJ, Lu Y, Danova NA, Kalscheur VL, Vanderby R, Markel MD, Muir P. Response of the osteocyte syncytium adjacent to and distant from linear microcracks during adaptation to cyclic fatigue loading. Bone. 2004; 35(4):881–891. [PubMed: 15454095]
22. Noble BS, Peet N, Stevens HY, Brabbs A, Mosley JR, Reilly GC, Reeve J, Skerry TM, Lanyon LE. Mechanical loading: Biphasic osteocyte survival and targeting of osteoclasts for bone destruction in rat cortical bone. Am. J. Physiol.-Cell Physiol. 2003; 284(4):C934–C943. [PubMed: 12477665]
23. Sun X, McLamore E, Kishore V, Fites K, Slipchenko M, Porterfield DM, Akkus O. Mechanical stretch induced calcium efflux from bone matrix stimulates osteoblasts. Bone. 2012; 50(3):581–91. [PubMed: 22227434]
24. De Groot K. Effect of porosity and physicochemical properties on the stability, resorption, and strength of calcium phosphate ceramics. Ann. NY Acad. Sci. 1988; 523:227–233. [PubMed: 3382123]
25. Shu R, McMullen R, Baumann MJ, McCabe LR. Hydroxyapatite accelerates differentiation and suppresses growth of MC3T3-E1 osteoblasts. J Biomed Materials Res A. 2003; 67:1196–1204.
26. Smith IO, McCabe LR, Baumann MJ. MC3T3-E1 osteoblast attachment and proliferation on porous hydroxyapatite scaffolds fabricated with nanophase powder. Int J Nanomed. 2006; 1:189–194.
27. McCabe LR, Banerjee C, Kundu R, Harrison RJ, Dobner PR, Stein JL, et al. Developmental expression and activities of specific Fos and Jun proteins are functionally related to osteoblast maturation: Role of Fra-2 and Jun D during differentiation. Endocrinology. 1996; 137:4398–4408. [PubMed: 8828501]
28. Harris L, Senagore P, Young V, McCabe LR. Inflammatory bowel disease causes reversible suppression of osteoblast and chondrocyte function in mice. Am J Physiol. 2009; 296(5):G1020–9.

29. Botolin S, McCabe LR. Chronic hyperglycemia modulates osteoblast gene expression through osmotic and non-osmotic pathways. J Cell Biochem. 2006; 99:411–424. [PubMed: 16619259]
30. Motyl KJ, Raetz M, Tekalur SA, Schwartz RC, McCabe LR. CAAT/enhancer binding protein beta-deficiency enhances type 1 diabetic bone phenotype by increasing marrow adiposity and bone resorption. Am J PhysiolRegulIntegr Comp Physiol. 2011 on line/in press.
31. Wang YH, Liu Y, Maye P, Rowe DW. Examination of mineralized nodule formation in living osteoblastic cultures using fluorescent dyes. BiotechnolProg. 2006; 22:1697–1701.
32. Tummers B. DataThief III manual v. 1.1. 2005:1–52.
33. Massey FJ. The Kolmogorov-Smirnov test for goodness of fit. J Am StatAssoc. 1951; 46:68–78.
34. Curray JR. The analysis of two-dimensional orientation data. J Geol. 1956; 64:117–131.
35. Fisher NI, Huntington JF, Jackett DR. Spatial analysis of two-dimensional orientation data. Math Geol. 1985; 17:177–194.
36. Lian JB, Stein GS, Stein JL, van Wijnen AJ. Osteocalcin gene promoter: Unlocking the secrets for regulation of osteoblast growth and differentiation. J Cell Biochem. 1998; 30-31:62–72.
37. Owen TA, Aronow M, Shalhoub V, Barone LM, Wilming L, Tassinari MS, et al. Stein GS. Progressive development of the rat osteoblast phenotype in vitro reciprocal relationships in expression of genes associated with osteoblast proliferation and differentiation during formation of the bone extracellular-matrix. J Cellular Physiol. 1990; 143:420–430. [PubMed: 1694181]
38. Quarles LD, Yohay DA, Lever LW, Caton R, Wenstrup RJ. Distinct proliferative and differentiated stages of murine MC3T3-E1 cells in culture – An in vitro model of osteoblast development. J Bone Miner. 1992; 7:683–692.
39. Bao Y, Liu L, Zhou Y. Assessing the elastic parameters and energy-dissipation capacity of solid materials: A residual indent may tell all. Acta Mater. 2005; 53:4857–4862.
40. Shahdad S, McCabe JF, Bull S, Rusby S, Wassell RW. Hardness measured with traditional Vickers and Martens hardness methods. Dent Mater. 2007; 23:1079–1085. [PubMed: 17141860]
41. Rouxel T, Sanglebouef J, Moysan C, Truffin B. Indentation topometry in glasses by atomic force microscopy. J Non-Cryst Solids. 2004; 344:26–36.
42. Anselme K. Osteoblast adhesion on biomaterials. Biomaterials. 2000; 21:667–681. [PubMed: 10711964]
43. Vlacic-Zischke J, Hamlet SM, Friis T, Tonetti MS, Ivanovski S. The influence of surface microroughness and hydrophilicity of titanium on the up-regulation of TGFβ/BMP signalling in osteoblasts. Biomaterials. 2011; 32(3):665–71. [PubMed: 20933273]
44. Zayzafoon M. Calcium/calmodulin signaling controls osteoblast growth and differentiation. J. Cell. Biochem. 2006; 97(1):56–70. [PubMed: 16229015]
45. Lee DH, Park BJ, Lee MS, Lee JW, Kim JK, Yang HC, et al. Chemotactic migration of human mesenchymal stem cells and MC3T3-E1 osteoblast-like cells induced by cos-7 cell line expressing rhBMP-7. Tissue Eng. 2006; 12:1577–1586. [PubMed: 16846353]
46. Frost HL. Presence of microscopic cracks *in vivo* in bone. Henry Ford Hospital Medical Bulletin. 1960; 8:27–35.
47. Stafford HJ, Roberts MT, Oni O, Hay J, Gregg P. Localization of bone-forming cells during fracture healing by osteocalcin immunocytochemistry: An experimental study of the rabbit tibia. J Orthop Res. 1994; 12:29–39. [PubMed: 8113940]
48. Spence G, Patel N, Brooks R, Rushton N. Carbonate substituted hydroxyapatite: Resorption by osteoclasts modifies the osteoblastic response. Journal of Biomedical Materials Research Part A. 2009; 90A(1):217–224. [PubMed: 18496864]
49. Beck GR. Inorganic phosphate as a signaling molecule in osteoblast differentiation. J Cell Biochem. 2003; 90:234–243. [PubMed: 14505340]
50. Morgan J, Holtman KR, Keller JC, Stanford CM. In vitro mineralization and implant calcium phosphate-hydroxyapatite crystallinity. Implant Dentistry. 1996; 5:264–271. [PubMed: 9206394]
51. Chang YL, Stanford CM, Keller JC. Calcium and phosphate supplementation promotes bone cell mineralization: Implications for hydroxyapatite (HA)-enhanced bone formation. J Biomed Mater Res. 2000; 52:270–278. [PubMed: 10951365]

52. Yang H, Curinga G, Giachelli CM. Elevated extracellular calcium levels induce smooth muscle cell matrix mineralization in vitro. Kidney Int. 2004; 66:2293–2299. [PubMed: 15569318]
53. Ducheyne P, Radin S, King L. The effect of calcium phosphate ceramic composition and structure on in vitro behavior. I. Dissolusion. J Biomed Mater Res. 1993; 27:25–34. [PubMed: 8380596]
54. Meleti Z, Shapiro IM, Adams CS. Inorganic phosphate induces apoptosis of osteoblast-like cells in culture. Bone. 2000; 27:359–366. [PubMed: 10962346]
55. Blair H, Robinson L, Huang CL, Sun L, Friedman P, Schlesinger P, Zaidi M. Calcium and bone disease. Biofactors. 2011; 37:159–67. [PubMed: 21674636]
56. Lawn B, Wilshaw R. Indentation fracture: principles and applications. J Mater Sci. 1975; 10(6): 1049–1081.
57. Zhang W, Submash G. Finite element analysis of interacting Vickers indentations on brittle materials. ActaMater. 2001; 49:2961–2974.
58. Wang W, Xuan F, Liang J, Wang L. Dissolution of plasma-sprayed wollastonite coatings: the effects of microstructure coupled with stress. ASM International. 2012; 21:908–916.
59. Shu Y, Case ED, Baumann MJ. Slow growth of microcracks in hydroxyapatite during aging. J Mater Sci. 2012; 47(18):6542–6552.
60. Evans AG, Hutchinson JW. On the mechanics of delamination and spalling in compressed films. Int. J. Solids Structure. 1984; 20(5):455–466.
61. Li D, Yang MX, Muralidhar P, Wu C, Yang F. Local surface damage and material dissolution in 45S5 bioactive glass: Effect of the contact deformation. J Non-Cryst Solids. 2009; 355:876–879.
62. Deligianni DD, Katsala ND, Koutsoukos PG, Missirlis YF. Effect of surface roughness of hydroxyapatite on human bone marrow cell adhesion, proliferation, differentiation and detachment strength. Biomater. 2000; (22-1):87–96.
63. Linez-Bataillon P, Monchau F, Bigerelle M, Hildebrand HF. In vitro MC3T3 osteoblast adhesion with respect to surface roughness of Ti6Al4V substrates. BiomolEng. 2002; (19-2-6):133–141.
64. Fuzzi M, Zaccheroni Z, Vallania G. Scanning electron microscopy and profilometer evaluation of glazed and polished dental porcelain. Int J Prosthodont. 1996; (9-5):452–458. [PubMed: 9108746]
65. Hutson AL, Niinomi M, Nicholas T, Eylon D. Effect of various surface conditions on fretting fatigue behavior of Ti-6Al-4V. Int J Fatigue. 2002; (24-12):1223–1234.
66. Lathabal S, Robel J, Dabbs T, Lawn BR. Fracture-mechanics model for subthreshold indentation flaws. 1. Equilibrium fracture. Journal of Materials Science. 1991; (26-8):2157–2168.

Highlights

- We introduced microcracks onto hydroxyapatite disk surfaces
- Osteoblast attachment and maturation increased on cracked versus non-cracked discs
- Osteoblasts preferentially aligned toward the indentation site at 75-90 μm radius
- Microcracks stimulate calcium release which may signal osteoblast attachment
- Microcracks can add a new dimension to scaffold design for bone tissue engineering

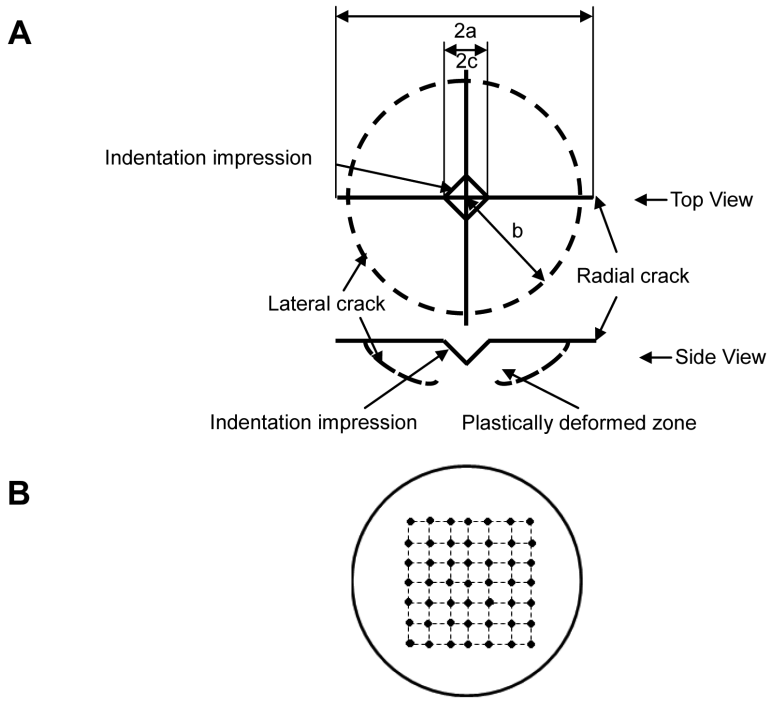

Figure 1. Diagram of radial crack introduction into HA specimens

(**A**) Radial cracks introduced by Vickers indentation at 4.91 N; (**B**) A 7×7 grid with a 2 mm interval indentation pattern on HA specimens.

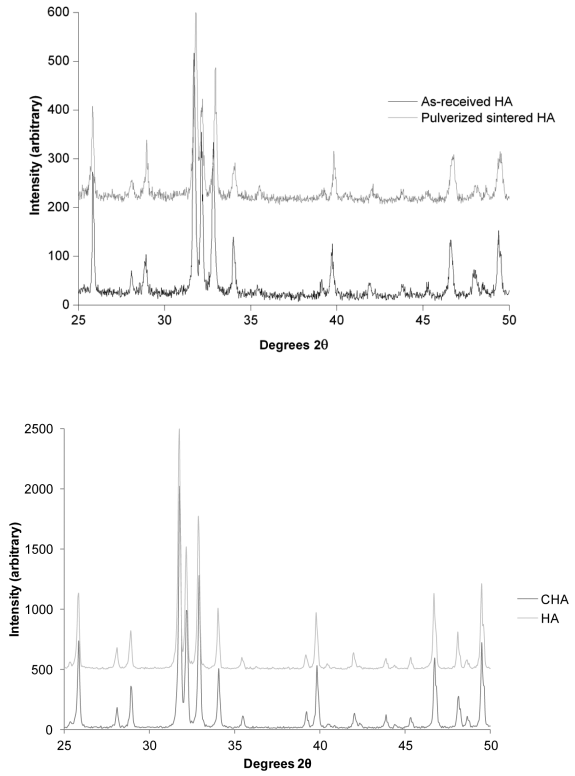

Figure 2. XRD spectra of HA

(*Above*) XRD spectra of as-received HA powder from vendor and pulverized sintered HA specimen. (*Below*) XRD of HA and CHA ground sintered powders used for OC study. All powders showed representative peaks for HA crystal and no impurity phases were detected.

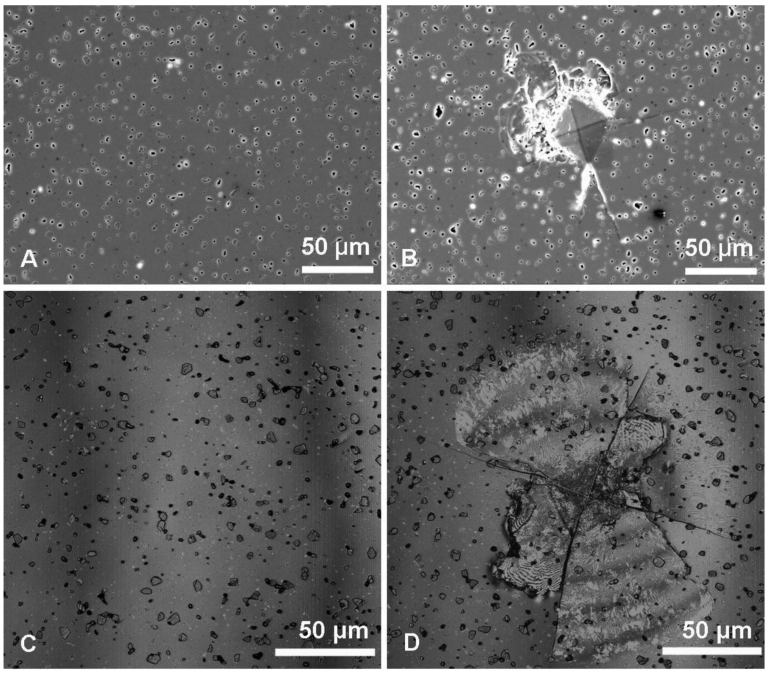

Figure 3.

SEM images of (**A**) polished non-microcracked HA surface and (**B**) microcracked HA surface and CLSM Z-stack maximum reflection intensity projections of (**C**) polished non-microcracked HA surface and (**D**) microcracked HA surface. On the microcracked HA surface, Vickers indentation impression is the center diamond shape. Accompanying radial cracks and lateral crack spalling are pointed out by white and black arrows, respectively.

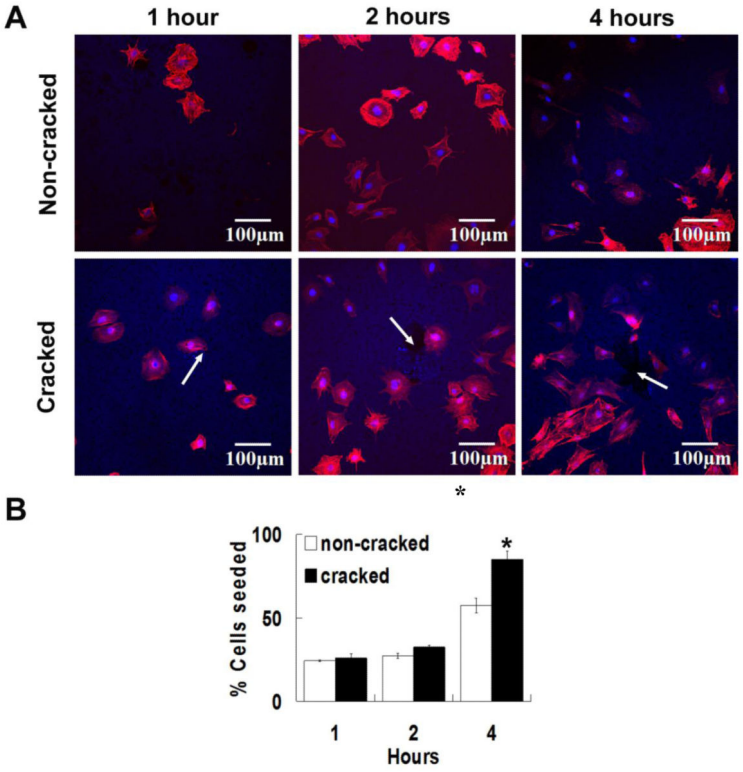

Figure 4. Osteoblast attachment to HA

(**A**) Cell attachment to non-microcracked and microcracked HA specimens at 1, 2 and 4 hours. White arrows show positions of Vickers indentations and cracks. The OBs were stained with Rhodamine Phalloidin (actin) and Hoescht 33342 (nucleus). The rhodamine phalloidin actin fluorescence stain was excited at 543 nm and emission was detected through a BA560-620 nm emission filter (represented in red). The Hoechst 33342 nucleus stain was excited with UV light at 405 nm and emission was detected through a BA430-470 emission filter (represented in blue). (**B**) Percentage of OB attachment to non-microcracked and cracked HA specimens at 1, 2 and 4 hours (relative to cells seeded). Error bars represent standard error. Data analyzed by student's t-test (*$p<0.05$). Three specimens were used for each condition and the experiments were tripled.

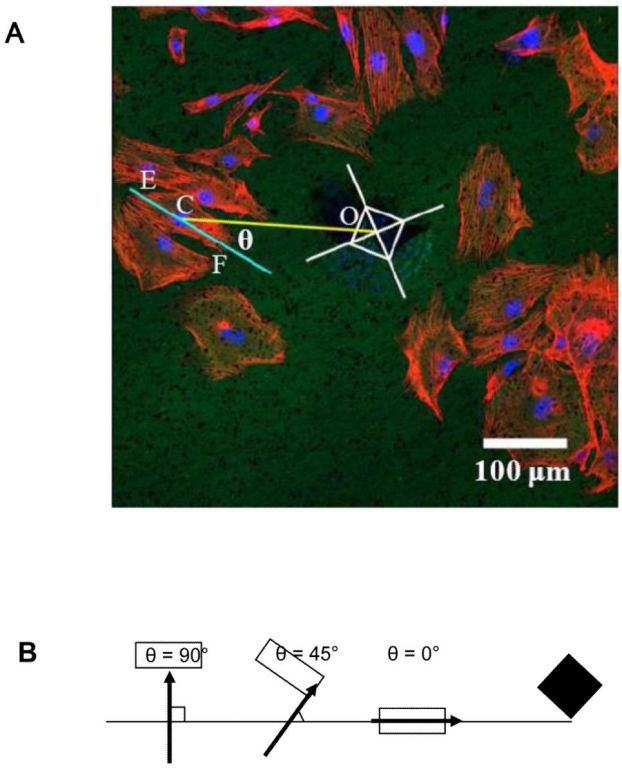

Figure 5. Illustration of cell attachment angles

(**A**) Micrograph of cell angle θ between cell elongation direction (cyan line EF) and line connecting cell nucleus (C) and indentation center (O) (yellow line OC) of microcracked HA. The indentation impression and radial crack pattern are illustrated by white lines. The black crosses mark examples of cells showing no apparent elongation direction. The OBs were stained with Rhodamine Phalloidin (Actin) and Hoescht 33342 (nucleus). (**B**) A schematic of cells with different elongation directions with respect to the indentation site (black diamond). Cells with $\theta < 45°$ are considered as aligned cells, while cells with $\theta \geq 45°$ are considered as non-aligned cells.

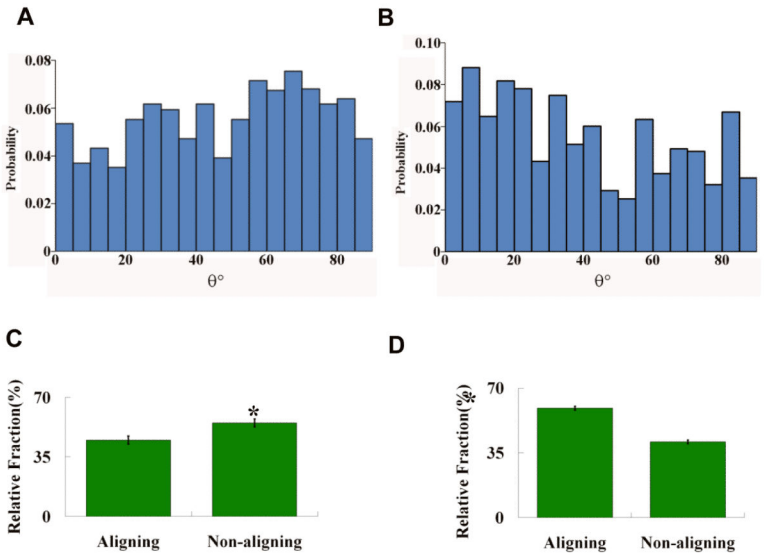

Figure 6. Probability and relative fraction of aligned cells on non-microcracked (A, C) and microcraked (B, D) HA

Top: Probability density histograms of cell alignment θ for (**A**) non-microcracked HA (N=489) and(**B**) microcracked HA (N=587) fit to uniform distribution as shown by the thick solid black line. N is the total number of cells considered in the probability density histograms. The goodness of fit was tested using the Kolmogorov-Smirnov method. The θ distribution for non-microcracked HA fitted to uniform distribution ($p>0.05$). The θ distribution for microcracked HA did not fit to the uniform distribution ($p<0.05$). *Bottom:* The relative fractions of aligned cells ($\theta<45°$) and non-aligned cells ($\theta \geq 45°$ and circular cells) on (**C**) non-microcracked HA and (**D**) microcracked HA at 4 hours. The significance of difference was detected using Student's t-test ($p<0.05$).

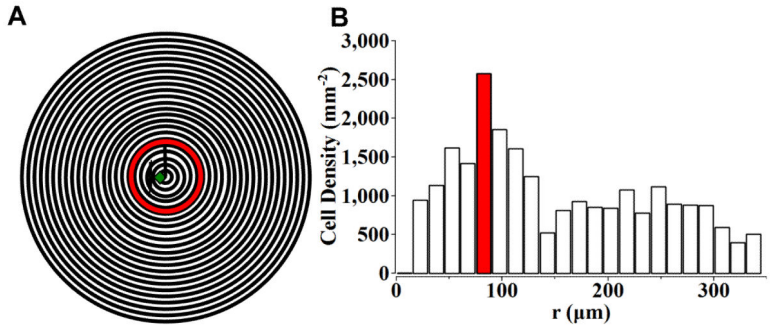

Figure 7. Osteoblast alignment based on distance from crack

The micrograph was partitioned into a central circle of 15 μm in radius and 15 μm wide outer rings (**A**). The number of OBs with aligned tendency (θ<45°) in the center circle and outer rings (15 μm wide) were counted and normalized by the area respectively (**B**). Most cells with aligned tendency (θ<45°) were found in the annulus 75 to 90 μm from the indentation center (**B**), which is around the tip of the radial cracks from Vickers indentation (**A**).

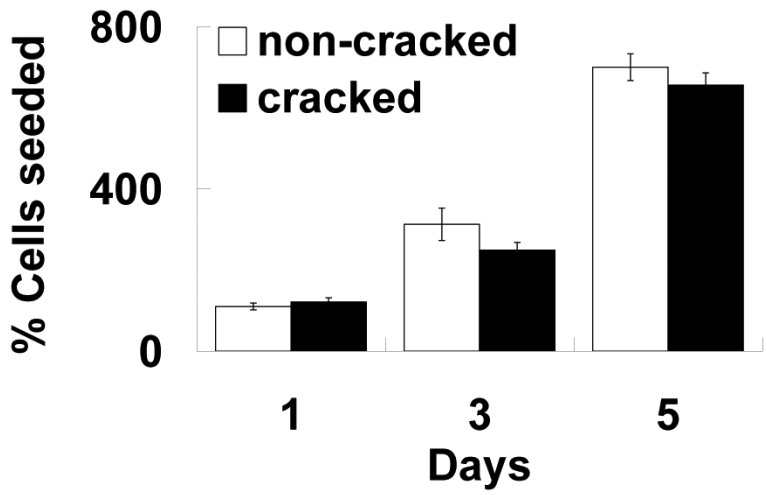

Figure 8. Osteoblast growth is not affected by the presence of cracks on HA specimens

OBs were seeded at an initial density of 11,320 cells/cm^2. OB growth on non-microcracked and microcracked HA specimens at 1, 3 and 5 days are represented by the relative percentage of cells seeded. Values are averages +/− SE. No significant differences were detected between non-microcracked and microcracked HA specimens (*$p<0.05$). Three specimens were used for each condition and the experiments were tripled.

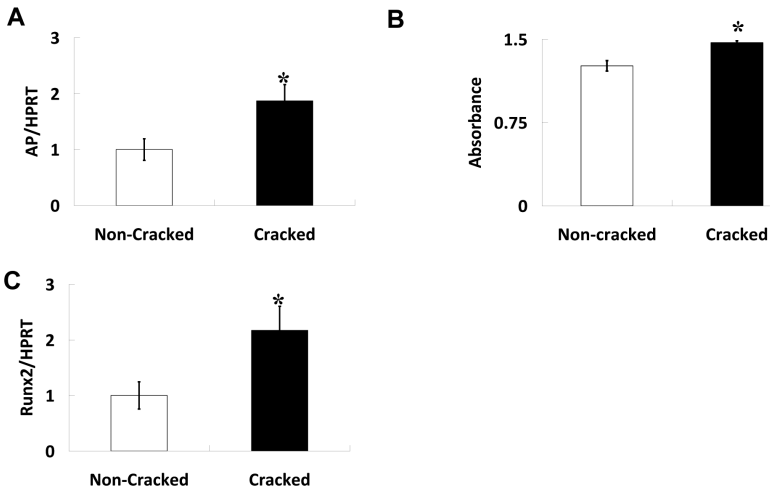

Figure 9.

HA microcracks enhance osteoblast maturation characterized by increased (**A**) Alkaline phosphatase (AP) activity and (**B**) AP and (**C**) runx2 mRNA levels. OBs were grown for 21 days on the specimens. RNA was extracted and expression of genes of interest was normalized to levels of an unmodified housekeeping gene, HPRT. AP activity was assessed on cell layers and then measured by spectrophotometer. Significant determined using Student's t-test (*$p<0.05$). Values are averages +/− standard error. Three specimens were used for each condition and the experiments were tripled.

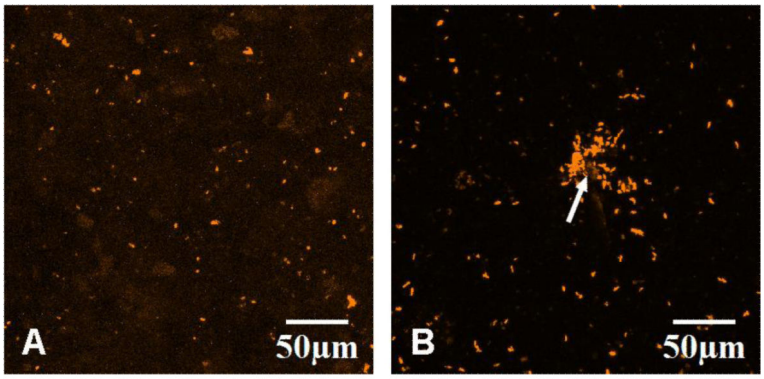

Figure 10.

CLSM Z-stack maximum fluorescence intensity projections of osteoblast mineral depositions on (**A**) non-microcracked and (**B**) microcracked HA at 21 days. The OBs were pulsed with Xylenol Orange every other day during culturing since day four. The Xylenol Orange fluorescence stain was excited at 543 nm and emission was detected through a BA560-620 emission filter (represented in orange).

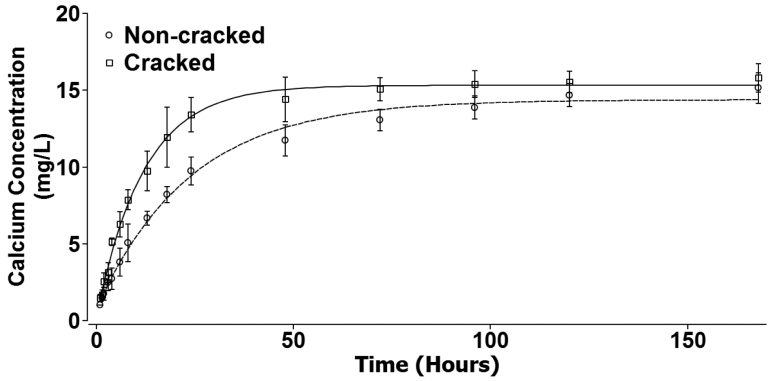

Figure 11.

The calcium ion concentrations released from non-microcracked (○) and microcracked (□) HA specimens as a function of time. Error bars represent standard deviations. Both the non-microcracked HA calcium release data and the microcracked HA calcium release data were fit to equation (4), which yielded a coefficient of determination $R^2 = 0.994$ and $R^2 = 0.996$, respectively.